Edinburgh Research Explorer

Fractional Frequency Reuse in DCO-OFDM-Based Optical Attocell Networks

Fractional Frequency Reuse in DCO-OFDM-Based Optical Attocell Networks

Cheng Chen, *Student Member, IEEE*, Stefan Videv, Dobroslav Tsonev, *Member, IEEE*,
and Harald Haas, *Member, IEEE*

Abstract—**In this paper a fractional frequency reuse (FFR) technique is considered in a direct-current optical orthogonal frequency-division multiplexing-based optical attocell network. An optical attocell network is proposed as a special type of visible light communication system that has the complete function of a cellular network. The cellular network is composed of many cells of extremely small size—the optical attocells. Two FFR schemes, strict fractional frequency reuse and soft frequency reuse, are considered. The signal-to-interference-plus-noise ratio (SINR) statistics and the spectral efficiency of the optical cellular system with FFR are analyzed. The performance of the systems with full frequency reuse and FFR is evaluated and compared. The results show that the FFR scheme can effectively achieve interference mitigation in an optical attocell network. The cell edge user SINR and spectral efficiency are significantly improved. Additionally, FFR provides improvements in average spectral efficiency. The effects of important parameters such as cell radius are also studied.**

Index Terms—**Cellular network, fractional frequency reuse, orthogonal frequency division multiplexing, visible light communications.**

I. INTRODUCTION

The level of data traffic in wireless communication networks has increased exponentially in the past two decades. If this trend continues in the future, the limited radio frequency (RF) spectrum will no longer meet the wireless data transmission demand [1]. One of the emerging solutions to this spectrum crisis is the migration of wireless communication techniques into the visible light spectrum due to its many promising advantages [2]. For example, visible light communication (VLC) can be embedded in the existing lighting infrastructure.

In a typical VLC system, a low-cost commercially available light emitting diode (LED) and photodiode (PD) can be used as the front-end devices [2]. Since an LED is an incoherent optical source, information is encoded using intensity modulation (IM). At the receiver side, the light intensity is converted to an electrical signal by a PD using direct detection (DD). A limiting factor of such an IM/DD system is the bandwidth of the LED and PD devices. Various techniques have been considered to

boost the transmission speed of VLC systems. Some researchers have explored the spatial diversity gain by using multiple-input multiple-output techniques [3], [4]. Advanced spectral efficient modulation techniques have also been considered [5], [6]. Another approach to improve the spectral efficiency of a wireless communication system is to increase the spatial reuse of the spectrum resources [7]. In many large indoor environments, multiple light fixtures are installed, and this provides the opportunity to set up a VLC system with dense spatial reuse of the limited modulation bandwidth. An optical attocell network uses each of the luminaries as a small base station (BS) or access point (AP) serving multiple wireless users within the illuminated area [8]. Such a cellular system would have an uplink connection to achieve full-duplexing and provide handovers to allow users to roam within the room or an entire building. This is similar to a RF femtocell network, but an optical attocell network uses smaller cell sizes.

Direct-current optical orthogonal frequency division multiplexing (DCO-OFDM) has been considered for optical attocell networks because of its advantages: i) it can eliminate the effect of the time dispersive channel with low complexity equalisation [5]; ii) adaptive power and bit loading can be used in an OFDM system, thus the available spectral resources can be used with their full potential [9]; iii) a multiple access scheme can be easily achieved in an optical attocell network by dividing time and frequency resources among multiple users, which in RF is known as orthogonal frequency division multiple access (OFDMA) [10].

Similar to other cellular systems, co-channel interference (CCI) is an important issue that affects the user performance in an optical attocell network. Interference mitigation techniques have been extensively researched for optical wireless systems. In [11], the use of static resource partitioning was proposed to avoid CCI in a cellular optical wireless system. In [12], an optical femtocell system was proposed, which uses different wavelengths in adjacent cells to avoid CCI. The methods used in these two studies effectively mitigate CCI. However, the loss in spectral efficiency is also significant. In [13], a self-organising interference coordination technique based on the busy-burst signalling was proposed for an optical wireless cellular system in an aircraft cabin environment. This method offers improvements both in cell edge user performance and in average spectral efficiency, but it requires additional overhead for the busy burst time slot.

The fractional frequency reuse (FFR) technique is a cost-effective approach to achieve interference mitigation in a cellular system. It maintains the balance between the average spectral

efficiency and cell edge user performance with low system complexity [14]. Over the past few years, the FFR technique has been studied for applications in RF cellular networks. The FFR scheme does not require precise instantaneous channel state information (CSI) and is of low computational complexity. There are two typical FFR schemes: ii) strict fractional frequency reuse (sFFR) and ii) soft frequency reuse (SFR) [15]. sFFR divides the whole frequency band into multiple protected sub-bands and one common sub-band. Cell centre users in each cell experience minor interference from nearby BS, so the common sub-band is assigned to them. Since cell edge users receive higher interference power, protected sub-bands are assigned to the cell edge users, and the sub-bands are arranged such that there is a minimum spatial reuse distance between them. The SFR applies an even shorter reuse distance compared to the sFFR scheme. In addition to the use of a different sub-band for cell edge users in each adjacent cell, the SFR scheme allows the centre users to take the sub-bands that are assigned to cell edge users in adjacent cells. To protect the cell edge users, the transmission power for cell edge users is typically higher than that for the cell centre users.

In [16], an optical AP using two LED sources with different beam-width is considered. A VLC cellular system using a SFR scheme based on such an AP is proposed. The corresponding bit error rate performance and the effect of changing LED beam-width is evaluated. In a previous study [17], an FFR scheme is considered in a VLC cellular system using adaptive LED arrays with specified LED orientations as APs. The simulation results show that the FFR scheme achieves effective interference mitigation and improves the spectral efficiency. However, the improvements reported in these studies result partly from the spatial diversity. In order to evaluate the benefit solely from FFR schemes, a more general case is presented in this paper. A VLC system with APs that only transmit using a LED luminary with Lambertian radiation pattern is considered. This paper presents a first analytical framework for the evaluation of FFR in a DCO-OFDM-based optical attocell network.

The remainder of this paper is organised as follows: the system model, including the light propagation model, network model, modulation and multiple access schemes is presented in Section II. The statistics of signal-to-interference-plus-noise ratio (SINR) and spectral efficiency for FFR schemes are analysed in Section III. The results are presented in Section IV and the effects of key parameters are discussed. Conclusions are given in Section V.

II. SYSTEM MODEL

In this study, a system level analysis is carried out to evaluate the performance of an optical attocell network. Since the transmission data rate is much faster than the channel variation due to user movement, users are considered to be quasi-static. In addition, this study focuses on the downlink performance of the system, so the effects on the system performance and the operation of handover schemes are outside the scope of this study. User equipment is placed at the desktop height where a typical height of 0.85 m is used. A PD receiver with a field
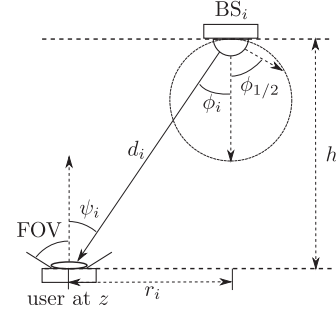

Fig. 1. LOS light propagation geometry.

of view (FOV) of 90° (full FOV) is mounted on the top of the user equipment. The FOV of the receiver is defined as the angle between the normal of the PD surface and the direction with the maximum incident angle to the receiver, which is illustrated in Fig. 1. The receiver is orientated upwards. All BS are mounted on the ceiling where a typical value for ceiling height of 3 m is used. The direction of the BS optical transmitter is vertically downwards.

A. Light Propagation Model

In order to estimate the signal power from a specified BS to a user, a propagation model is necessary to calculate the path loss. The dominant transmitted signal component in this system is the light through the line-of-sight (LOS) path. This channel can be modelled using the direct-current (dc) channel gain. The corresponding two-dimensional (2-D) geometry is shown in Fig. 1. The dc gain from the ith BS to the observed user can be calculated as [18]:

$$G_i = \frac{(m+1)A_{\mathrm{pd}}}{2\pi d_i^2} \cos^m(\phi_i)\cos(\psi_i),$$

where m denotes the Lambertian emission order which is given by $m = -\ln(2)/\ln(\cos(\phi_{1/2}))$ in which $\phi_{1/2}$ is the half-power semi-angle of the LED; A_{pd} is the physical area of the receiver PD; d_i denotes the Euclidean distance between BS_i and the user; ϕ_i denotes the corresponding light radiance angle; and ψ_i is the corresponding light incidence angle. The optical source has a half-power semi-angle $\phi_{1/2}$ of 60°, which is sufficient for a diffused luminary. The variables d_i, ϕ_i and ψ_i can be rewritten as a function of r_i by using $\cos(\phi_i) = \cos(\psi_i) = \frac{h}{d_i}$ and $d_i = \sqrt{r_i^2 + h^2}$. As shown in Fig. 1, r_i refers to the horizontal separation between the user and the ith BS. The LOS transmission model can then be converted to a function of r_i as:

$$G_i(r_i) = \frac{(m+1)A_{\mathrm{pd}}h^{m+1}}{2\pi}\left(r_i^2 + h^2\right)^{-\frac{m+3}{2}}. \qquad (1)$$

Occasionally, the LOS path may be shadowed or completely blocked. In these cases, a user may need an alternative serving BS or rely on a diffused link. Due to the modelling complexity and the limited space in this paper, these issues are treated as special cases for future study. Therefore, we assume that shadowing and non-LOS transmission issues are outside the scope of this work.
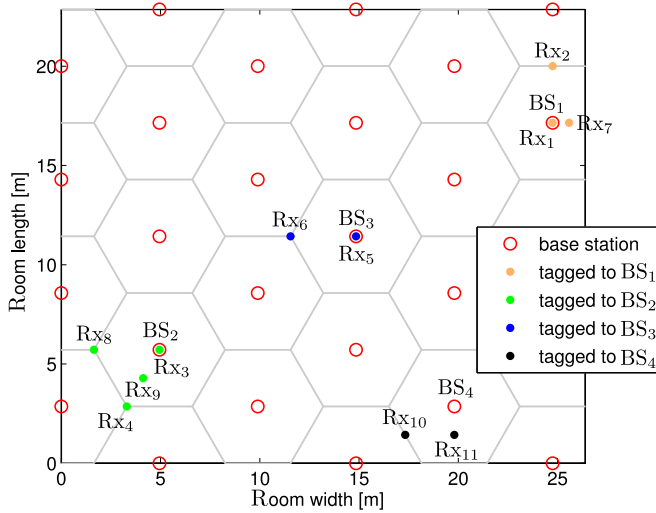
Fig. 2. An optical attocell network embedded in a large room of size 23 m × 26 m × 3 m. The number of cells is 27. The cell radius $R = 3.3$ m and the cell radius definition is shown in Fig. 7.

Fig. 3. Normalised channel gain against frequency. The corresponding receiver locations are shown in Fig. 2.

In addition to the LOS transmission, light from reflections (mainly from walls, ceiling and floor) causes multipath distortion to the optical channel. In order to observe this multi-path distortion effect, information about the channels considering multi-path reflection is required. An effective way to estimate this information is by using the multi-path ray-tracing simulation [19] to generate the channel data. However, it is time-consuming and difficult to show cases for all indoor environments and all user positions. Therefore, a number of examples are demonstrated to reflect the typical and worst cases. In these examples, the simulated environment is a large empty room of size 23 m × 26 m × 3 m. The room size is related to the cell size and the number of cells in the network. The optical source of each BS has a half-power semi-angle $\phi_{1/2}$ of $60°$, which is sufficient for a diffused luminary. The reflectivity of walls and the ceiling is 0.7, and the reflectivity of the floor is 0.3. Reflected signal components up to the third order are considered in the simulation. The network deployment and the user receiver positions are shown in Fig. 2. Each user in the room is served by the closest BS. Among all of the tessellating shapes, a hexagon cell shape shows a reasonable approximation to a circle [20]. Therefore, the hexagonal network deployment is preferred in the modelling of the cellular network. In this initial performance evaluation of a VLC based cellular system, it is intuitive to adopt the same network deployment.

Based on the method introduced in [19], the initial generated data are in the form of impulse responses. It is observed from these impulse responses that the overall signal power contribution from wall reflections is not as significant as those shown in [19] due to the large size of the considered room. Furthermore, the contribution from the third and higher order reflections is negligible due to the significant path loss and absorptions. The second order reflection generally corresponds to the reflections between floor and ceilings, and contributes significantly to the reflected signal power. The first order reflection corresponds to the reflections by the walls to the receiver. Its significance
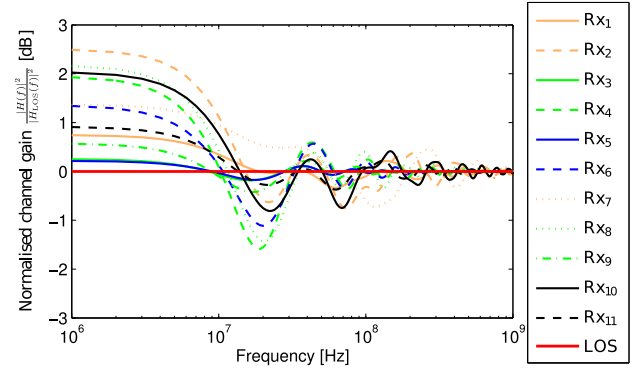
strongly depends on whether the transmitter and the receiver is close to one or more walls of the room. When a user is in the edge of the room, the first order reflection contributes significantly to the reflected signal. Therefore, the channel frequency response of the users in the room edge would be the worst case due to wall reflections. The channels corresponding to 'Rx$_5$' and 'Rx$_6$' are in the centre of the room as shown in Fig. 2. Their performance would reflect the typical channel characteristics in an optical attocell network. The user positions for the remaining nine channels are in the edge of the room, which would reflect the characteristics of the worst case channel.

It is important to assess whether the channel is flat in a wide frequency range, and therefore the simulated results are shown in the form of channel gain calculated as a function of frequency $|H(f)|^2$. Conventionally, the channel gain is normalised with the channel gain at dc. In this study, two cases are compared: with, and without the reflected signal. In order to highlight the difference, the channel gain is normalised by the channel gain with only a LOS component. The normalised channel gain is calculated by $\frac{|H(f)|^2}{|H_{LOS}(f)|^2}$. The result is shown in Fig. 3.

With an increase of frequency, all of the normalised channel gains fluctuate around 0 dB (channel gain with LOS only). The variation of the fluctuation is less than 3 dB. In addition, for users that are further away from the room edges, due to the lower significance of the first order reflection, the channel gain variation with frequency is less significant compared with the room edge user case. For example, the channel gain variation for Rx$_5$ and Rx$_6$ are less than 1.5 dB as shown in Fig. 3. The maximum achievable signal-to-noise ratios (SNRs) in many VLC experiments are around 30 dB [9], [21], [22]. However, the received SNR decreases when the user is away from the cell centre due to a larger path loss. In order to ensure that the system is not limited by the receiver noise, the considered systems in this study are configured to have a worst case SNR (user at cell edge) of more than 10 dB. In the case of a SNR of 10 dB, uncoded four-quadrature amplitude modulation is used, which requires a minimum SNR of about 10 dB. Therefore, compared with the considered SNR range of 10 to 30 dB, the variation in channel gain is minor. In addition, the effect of adding reflected signals offers extra channel gain at some frequencies while it decreases the channel gain at other frequencies. On average, adaptive bit
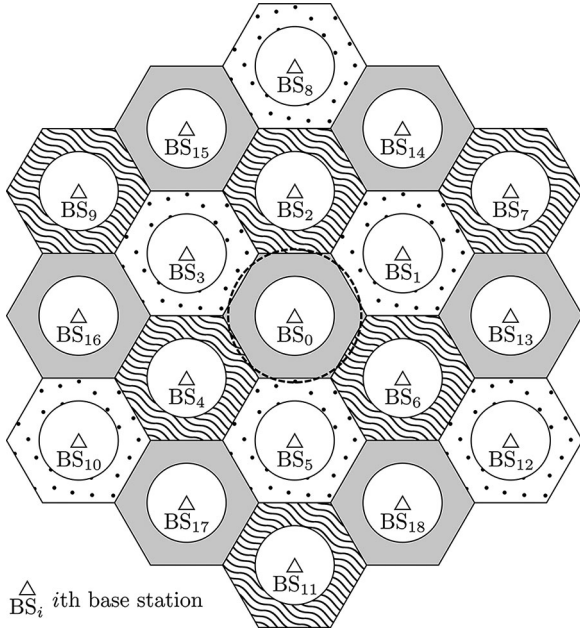
Fig. 4. Two-layer optical attocell network model with 19 cells. The patterns in the edge regions of every cells demonstrate the FR pattern for the FFR schemes, and the corresponding reuse factor is 3.

Fig. 5. The 2-D spatial distribution of $\mathcal{D}$ in the deployed networks with different network sizes. (a) $11.4 \text{ m} \times 13.2 \text{ m}$ room with seven cells. (b) $14.3 \text{ m} \times 16.5 \text{ m}$ room with 12 cells. (c) $17.1 \text{ m} \times 19.8 \text{ m}$ room with 17 cells. (d) $22.9 \text{ m} \times 26.4 \text{ m}$ room with 27 cells. The used cell radius is $R = 3.3$ m.

loading in OFDM can compensate for the variation in channel gain. Therefore, approximating the frequency domain channel gain to be flat would not cause significant inaccuracy in the analysis. The reason for this minor multi-path distortion is the dominance of the LOS in the channel. When the Rician factor is high enough, the channel gain can be approximated to be flat in the frequency domain [23]. Therefore, the multi-path effect caused by wall reflections is assumed to be negligible and can be mitigated by OFDM [24] in this study.

B. Cellular Network Model

When evaluating the user performance in the room shown in Fig. 2, the serving BS changes depending on the position of a user. In addition, for users in different cells, the set of interfering BS is different. Furthermore, the coverage area of cells in the edge of the room is part of a hexagon. All of these factors mean that it is complex to analyse the system performance. Therefore, an alternative simplified model is considered to estimate the performance of a realistic system. Here, a network which extends to infinity in the 2-D plane is considered. In this case, the layout of the interfering BS and the cell shape would be identical for the users in any cell. As the interference is generally dominated by the closest interfering BS, the interference from BS further away from the user is not considered for simplicity. Thus, a two-layer hexagonal network model shown in Fig. 4 is used to analyse the user performance. In this two-layer network model, 19 BS with index i are considered, where $i = 0, \ldots, 18$. The performance of the users in the central cell served by the 0th BS is evaluated to estimate the performance of users in the network deployed in a room. For the convenience of description, the network deployed in a room is termed as a 'deployed network' in the remainder of this paper. Some of the neighbouring
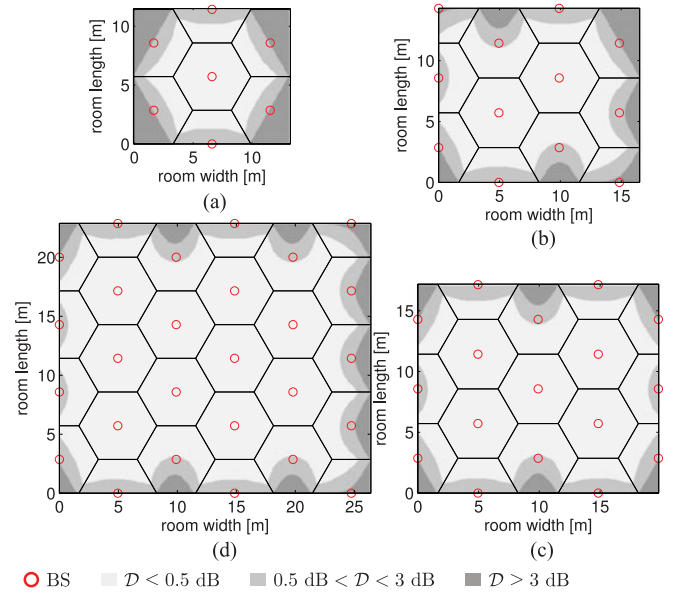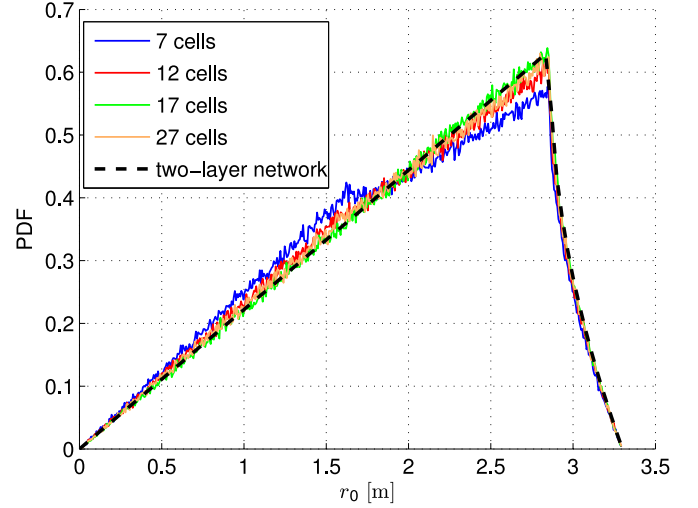
Fig. 6. Statistics of the horizontal separation between the serving BS and the user in different networks. 'two-layer network' refers to the results for the two-layer network model. '7 cells', '12 cells', '17 cells' and '27 cells' refer to the results for the deployed networks with different network sizes. The corresponding network deployments are shown in Fig. 5.

BSs cause interference to the users in the central cell. Whether the ith BS causes interference depends on the reuse scheme in the system.

Despite the difference in the user performance in the two-layer network model and the deployed networks, the results shown in Figs. 5 and 6 demonstrate that this is minor. Firstly, the closer the considered cell is to the room edge, the less the number of interfering BS to the users. Consequently, it would seem that the two-layer network model only offers a good estimation to the user performance in the cells in the room central area. However, as mentioned above, the interference is dominated by the closest interfering BS. Even if the user is in the cell in the edge

TABLE I
INTERFERENCE LEVEL DIFFERENCE

number of cells	7	12	17	27
$\mathcal{D} < 0.5$ dB	48%	64%	76%	77%
$\mathcal{D} < 3$ dB	75%	89%	95%	94%

of the room, as long as it is close to the cell edge towards the room centre, the received interference should be close to that received in the two-layer network model. To demonstrate the accuracy of the interference estimation by using the two-layer network model, simulations of the 2-D spatial distribution of the interference power in the deployed networks with full frequency reuse (FR) are carried out. In addition, the interference power estimated by using the two-layer network model in all positions in the deployed network is calculated and compared to the simulated interference. The interference calculation is based on (1). The interference in the deployed network is defined as $\tilde{\mathcal{I}}$. The interference estimated for the two-layer network model is defined as $\mathcal{I}$. The difference between $\tilde{\mathcal{I}}$ and $\mathcal{I}$ is defined as $\mathcal{D} = |10\log_{10}(\tilde{\mathcal{I}}/\mathcal{I})|$. A lower value of $\mathcal{D}$ indicates a better approximation of the interference by using the two-layer network model. The spatial distributions of $\mathcal{D}$ in rooms with 7, 12, 17 and 27 cells are shown in Fig. 5. It shows that a significant interference difference occurs only in the room edges. The notable results are summarized in Table I, and it shows that the proportion of the area showing significant deviation in the interference estimation decreases with an increase of the number of cells in a room. In the case of 27 cells, 77% of the area has $\mathcal{D}$ lower than 0.5 dB and 94% of the area has $\mathcal{D}$ lower than 3 dB. In other words, the interference level is poorly estimated by the two-layer network model in only 6% of the room area. Since a large number of deployed cells is the typical case in an optical attocell network, the two-layer network model is considered to offer good approximation in terms of interference.

In addition, due to the limitation of the room edge, the non-hexagon cells in the edge of the room cause a deviation in the statistics of the path loss corresponding to the transmission of the desired signal in the deployed network from the case in the two-layer network model. In order to evaluate this difference, the empirical statistics of r_0 based on random user locations in different cases are simulated and compared. The random location of users follows a Possion point process (PPP). As described in Section II-A, r_0 refers to the horizontal separation between the user and the 0th BS in the two-layer network model. For the deployed network, r_0 refers to the horizontal separation between the user and its serving BS. It can be observed in Fig. 6 that the difference between the probability density function (PDF) of r_0 in a deployed network and that in the two-layer network model diminishes with an increase of the number of cells in the deployed network. Except for the case with 7 cells, the PDFs of r_0 in the deployed network shows a close agreement with that in the two-layer network model. Therefore, the performance in the two-layer network is considered to be a reasonable estimation of the deployed network. The estimation accuracy is
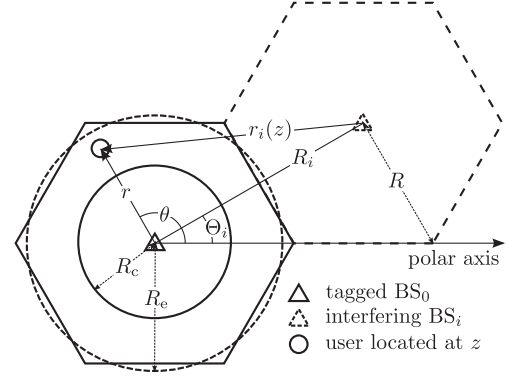

Fig. 7.   Geometric model with polar coordinates.

also demonstrated in the SINR results in Section IV as shown in Fig. 10.

In the two-layer network model, the coverage area of each cell is divided into a cell central area and a cell edge area as shown in Fig. 4. In order to further simplify the analysis, a circular cell approximation is applied to the considered central cell as shown in Fig. 7. The radius of the hexagonal cell is defined as R. The approximated circular cell has the same coverage area as the original hexagonal cell. Therefore, the equivalent radius of the circular cell is defined as $R_e \approx 0.91R$. In the system using FFR, the radius of the central area is defined as R_c. A parameter $\delta = \frac{R_c}{R_e}$ is defined to determine the size of cell central and edge area. For the convenience of the analysis in Section III, the indices of the 18 nearby BS are grouped into three sets based on the reuse pattern shown in Fig. 4. They include $I_A = \{13, 14, 15, 16, 17, 18\}$, $I_B = \{2, 4, 6, 7, 9, 11\}$ and $I_C = \{1, 3, 5, 8, 10, 12\}$. Note that the edge users in the 0th cell reuse the same spectral resources as those in I_A in the FFR systems.

The location of a user and interfering BS are defined using a 2-D polar coordinate system. The origin of the coordinates is placed at the location of BS_0. The orientation of the polar axis is shown in Fig. 7. The location of a user in the central cell is defined by $z = (r, \theta)$, where r is the horizontal separation between the user and the origin and $r \in [0, R_e]$; and θ is the polar angle of the user and $\theta \in [0, 2\pi)$. The location of the ith BS is defined in a similar way as (R_i, Θ_i), where R_i is the horizontal separation between BS_i and the origin, and Θ_i is the polar angle of BS_i. Since the network deployment and the cell radius R are given, the values of (R_i, Θ_i) are fixed and can be readily calculated. In order to estimate the signal power from BS_i to the observed user, the horizontal separation between BS_i to the user at z is essential, which is defined as $r_i(z)$. For $i = 0$, $r_0(z) = r$. The observed user, the serving BS, and the interfering BS_i form a triangle in the case of $i \neq 0$, $r_i(z)$ can be calculated using the rule of cosine as:

$$r_i(z) = \sqrt{r^2 + R_i^2 - 2R_i r \cos(\theta - \Theta_i)}.$$

C. DCO-OFDM and Multiple Access

The application of optical-OFDM can be extended to an OFDMA system to realise multiple access in an optical atto-cell network. Due to the relatively high spectral efficiency of

DCO-OFDM, this modulation scheme is used in this study. In an OFDM frame, the K frequency domain quadrature amplitude modulated data symbols before the inverse discrete Fourier transform (IDFT) are defined as: $X = [X_0 \; X_1 \; X_2 \; \cdots \; X_{K-1}]$. Since an intensity modulated signal is a real-value signal, Hermitian symmetry is required to make the OFDM symbols contain only real samples. This requires $X_k = X_{K-k}^*$, where $[\cdot]^*$ is the complex conjugate operation. In addition, X_0 and $X_{K/2}$ are set to zero [6]. Consequently, only $\tilde{K} = K/2 - 1$ symbols carry information. Also, the intensity modulated signal is unipolar. In order to avoid negative samples, a dc-bias is required. After carrying out the K-point IDFT and the addition of a dc-bias, the time domain OFDM symbol can be calculated as:

$$x(t) = x_{\mathrm{DC}} + \sum_{k=0}^{K-1} x_k(t), \; t = 0, 1, \ldots, K-1,$$

$$x_k(t) = \frac{X(k)}{\sqrt{K}} \exp\left(\frac{2\pi jkt}{K}\right),$$

where x_{DC} is the dc-bias; $x_k(t)$ represents the signal component which accounts for the modulated symbol on subcarrier k at time slot t; and j is the imaginary unit. After the addition of dc-bias, the remaining negative samples are set to zero. According to the results of the simulated channel impulse responses noted in Section II-A, no significant signal is received when the delay exceeds 50 ns. If a sampling frequency of 40 MHz is used, the length of the cyclic-prefix (CP) is only two OFDM symbols. Since the required CP length is short, the effect of adding a CP is omitted in this study. In a multiple access version of DCO-OFDM, the $\tilde{K}$ transmission channels (subcarriers) are shared by a number of users. In the FFR schemes, these subcarriers are divided into multiple sub-bands. Then the subcarriers in each sub-band are distributed to users who are permitted to use that sub-band for data transmission. Assuming perfect sampling and synchronization, the intensity modulated sample received at time slot t on subcarrier k can be expressed as:

$$y_k(t) = x_{0,k}(t)G_0 R_{\mathrm{pd}} + \sum_{i \in \textit{И}} x_{i,k}(t) G_i R_{\mathrm{pd}} + z_k(t), \quad (2)$$

where $x_{i,k}(t)$ is the transmitted signal sample from BS_i on subcarrier k at time slot t. In the case of $i = 0$, $x_{0,k}(t)$ is the transmitted signal sample for the desired user; R_{pd} denotes the responsivity of the PD and $z_k(t)$ represents the user receiver noise on subcarrier k. The second term of y_k accounts for the received interference signal, where $\textit{И}$ is the set of all the interfering BS. The receiver noise is modelled as an additive white Gaussian noise with noise power spectral density of N_0. Therefore, z_k is drawn from a Gaussian distribution with zero mean and variance of $\sigma_k^2 = N_0 W/K$, where W is the total IM bandwidth. Clipping noise and non-linearities are crucial when there is a requirement to minimise the output power of the transmitter. However, it is assumed that the high output power of the BS is sufficient for the indoor lighting function in this study. In other words, there is enough margin for the minimisation of b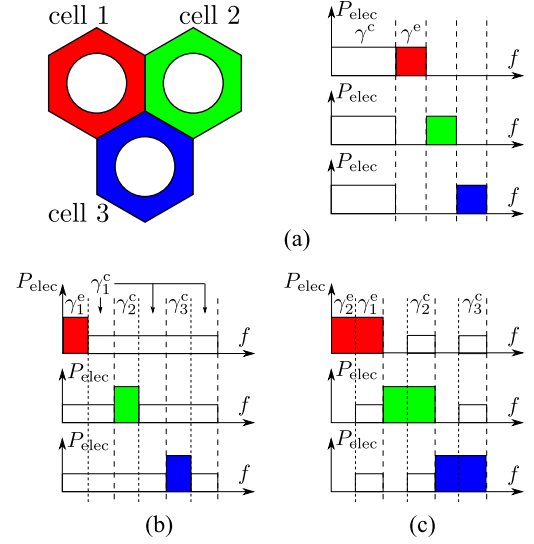oth effects by increasing the clipping threshold [25] and applying pre-distortion techniques [26]. Thus, clipping noise and non-linearities are not considered in this study.

Fig. 8. (a) sFFR. (b) SFR with $\delta^2 > \frac{2}{3}$. (c) SFR with $\delta^2 < \frac{2}{3}$.

D. FFR Schemes

In a FFR system, the serving BS needs to know whether the user is in the cell centre or is in the cell edge. This can be simply realised by determining the average signal strength of the downlink pilot signal. If the pilot signal power is higher than a threshold, this particular user is categorized as a cell centre user. Otherwise, the user is categorized as a cell edge user. It is assumed there is no movement of users within the period between two adjacent pilot signal transmissions. In the following frequency plan, subcarriers in each sub-band are equally distributed to the corresponding users for simplicity and user fairness.

1) Strict FFR: The considered sFFR divides the whole frequency band to three protected sub-bands and an individual common sub-band as shown in Fig. 8(a). The number of subcarriers of each sub-band is set to be proportional to the area of the central or edge regions, which offers good fairness and optimal performance [15]. The common sub-band is reused by the centre users in each cell. As shown in Fig. 8(a), one of the three protected sub-bands is assigned to the edge users of each cell. This assignment also ensures that the same protected sub-band is not reused in adjacent cells. Therefore, the number of subcarriers assigned to the cell centre users K_c and the number of subcarriers assigned to the cell edge users K_e are given as:

$$K_c = \left\lceil \tilde{K}\delta^2 \right\rceil,$$

$$K_e = \left\lfloor (\tilde{K} - K_c)/3 \right\rfloor,$$

respectively.

2) Soft Frequency Reuse: In SFR, the protected sub-bands for cell edge users are also reused in adjacent cells. In order to guarantee the performance of the cell edge users, the transmission power for the cell edge user is increased with a gain of β.

In addition, the different groups of subcarriers are assigned to edge users in adjacent cells. Similar to the sFFR scheme, for fairness, the number of subcarriers assigned to different user groups is proportional to the corresponding area. Therefore, the following frequency plan is used:

$$K_{\mathrm{c}} = \left\lceil \tilde{K} \delta^2 \right\rceil,$$

$$K_{\mathrm{e}} = \min \left(\left\lceil \tilde{K}/3 \right\rceil, \tilde{K} - K_{\mathrm{c}} \right),$$

which is shown in Fig. 8(b) and (c). Note that the maximum available bandwidth for cell edge users is $\tilde{K}/3$ to ensure the orthogonality of the protected sub-bands.

III. ASSESSMENT OF SINR AND SPECTRAL EFFICIENCY

Electrical SINR is an important metric to measure the quality of a wireless connection. Similar to the definition of SNR in an IM/DD optical wireless communication system, SINR is defined as the ratio of the received desired signal electrical power to the summation of noise and interference electrical power. Based on the SINR level, the spectral efficiency can be estimated in order to evaluate the wireless capacity of the system.

A. Full Frequency Reuse

1) Signal-to-Interference-Plus-Noise Ratio: The most straightforward frequency plan is FR, which reuses the whole frequency band in each cell. Here Δ is used to represent the reuse factor. In this case the reuse factor equals one ($\Delta = 1$). In this study, the FR system is used as the benchmark system. According to (2), the SINR of the user at location z on subcarrier k can be written as:

$$\gamma_{\mathrm{FR},k}(z) = \frac{P_{\mathrm{elec},0,k} G_0^2(z) R_{\mathrm{pd}}^2}{\sum_{i \in \mathit{H}} P_{\mathrm{elec},i,k} G_i^2(z) R_{\mathrm{pd}}^2 + \sigma_k^2}, \qquad (3)$$

where $P_{\mathrm{elec},i,k}$ denotes the electrical signal power transmitted by BS_i on subcarrier k, which is calculated as:

$$P_{\mathrm{elec},i,k} = \mathbb{E}\left[x_{i,k}^2(t) \right],$$

where $\mathbb{E}[\cdot]$ represents the expectation operation. Since $\Delta = 1$, the set $\mathit{H} = \mathit{H}_{\mathrm{A}} \cup \mathit{H}_{\mathrm{B}} \cup \mathit{H}_{\mathrm{C}}$. To simplify the analysis, an equal electrical power allocation is used. Assuming a total electrical transmission power of $P_{\mathrm{elec,AC}}$, $P_{\mathrm{elec},i,k} = P_{\mathrm{elec,AC}}/(K - 2)$. Then, the subscript k can be dropped and (3) can be modified as a function of z as:

$$\gamma_{\mathrm{FR}}(z) = \frac{(r^2 + h^2)^{-m-3}}{\sum_{i \in \mathit{H}} (r_i^2(z) + h^2)^{-m-3} + \Omega}, \qquad (4)$$

$$\Omega = \frac{4\pi^2 (K-2) N_0 W \kappa^2}{K P_{\mathrm{opt}}^2 (m+1)^2 A_{\mathrm{pd}}^2 R_{\mathrm{pd}}^2 h^{2m+2}}. \qquad (5)$$

The derivation of (4) and (5) is shown in Appendix A. Based on (4), the probability $\mathbb{P}[\gamma_{\mathrm{FR}} < T]$ can be calculated, where T is the threshold value.

2) SINR Statistics: In this study, a semi-analytical method is used to calculate the SINR statistics of the optical attocell systems. Assuming a polar angle of θ, the function of the SINR

on a subcarrier is monotonically decreasing with respect to r in the region of interest. Therefore, the conditional PDF of SINR can be calculated by using the PDF transformation rule as:

$$f_\gamma(\hat{\gamma}, f(r)|\theta) = \left. \frac{f(r)}{\left| \frac{\partial}{\partial r} \gamma(z) \right|} \right|_{r = \gamma^{-1}(\hat{\gamma}|\theta)},$$

where $f(r)$ is the PDF of r; $f(r)$ is determined by the locations of the considered users (cell edge/centre users); $\gamma^{-1}(\hat{\gamma}|\theta)$ is the inverse function of the SINR function with respect to r for a given θ, in which $\gamma(r_{\max}, \theta) \le \hat{\gamma} \le \gamma(r_{\min}, \theta)$. Here, $r_{\max}$ ($r_{\min}$) is the maximum (minimum) of r in its feasible region. A closed form solution to $\gamma^{-1}(\hat{\gamma}|\theta)$ is unavailable. Numerical methods are used to compute the function. Then the cumulative density function (CDF) of SINR can then be calculated as follows:

$$\mathbb{P}[\gamma < T] = \int_0^{2\pi} \int_{-\infty}^{T} f_\gamma(\hat{\gamma}, f(r)|\theta) \mathrm{d}\hat{\gamma} f_\theta(\theta) \mathrm{d}\theta. \qquad (6)$$

Since the spatial location of the users in each cell follows a PPP, the PDF of θ should follow: $f_\theta(\theta) = \frac{1}{2\pi}$. This semi-analytical approach is presented in [27] in detail.

In the case of the FR scheme, the statistics in the whole cell is calculated. Therefore, the PDF $f(r)$ is given as:

$$f(r) = f_r(r) = \frac{2r}{R_{\mathrm{e}}^2}, r \in [0, R_{\mathrm{e}}].$$

In the case of FFR systems, statistics in part of the cell is required. In the calculation of $\mathbb{P}[\gamma < T | r < R_{\mathrm{c}}]$ and $\mathbb{P}[\gamma < T | r \ge R_{\mathrm{c}}]$, the PDF $f(r)$ should be calculated as:

$$f_{r|r<R_{\mathrm{c}}}(r) = \frac{f_r(r)}{\mathbb{P}[r < R_{\mathrm{c}}]}, r \in [0, R_{\mathrm{c}}],$$

$$f_{r|r\ge R_{\mathrm{c}}}(r) = \frac{f_r(r)}{\mathbb{P}[r \ge R_{\mathrm{c}}]}, r \in [R_{\mathrm{c}}, R_{\mathrm{e}}],$$

where $\mathbb{P}[r < R_{\mathrm{c}}]$ ($\mathbb{P}[r \ge R_{\mathrm{c}}]$) is the probability that the user is in the cell central (edge) area. It is shown in [28] that:

$$\mathbb{P}[r < R_{\mathrm{c}}] = \delta^2,$$

$$\mathbb{P}[r \ge R_{\mathrm{c}}] = 1 - \delta^2.$$

3) Spectral Efficiency: In this study, the Shannon-Hartley formula is used to estimate the wireless capacity of the system. In a DCO-OFDM system, the spectral efficiency of a user at z can be calculated as a function of $\gamma(z)$ and Δ:

$$\rho(\gamma(z), \Delta) = \frac{K-2}{2K\Delta} \log_2(1 + \gamma(z)).$$

The average spectral efficiency for the users in the whole cell can be calculated as:

$$\bar{\rho} = \mathbb{E}_z[\rho(\gamma(z), \Delta)],$$

$$= \int_0^{2\pi} \int_0^{R_{\mathrm{e}}} \rho(\gamma(r, \theta), \Delta) f_r(r) \mathrm{d}r f_\theta(\theta) \mathrm{d}\theta. \qquad (7)$$

In addition, the average spectral efficiency for the users in the cell centre area can be calculated as:

$$\bar{\rho}^{\mathrm{c}} = \mathbb{E}_z[\rho(\gamma(z), \Delta) | r < R_{\mathrm{c}}],$$
$$= \int_0^{2\pi} \int_0^{R_{\mathrm{c}}} \rho(\gamma(r, \theta), \Delta) f_{r|r<R_{\mathrm{c}}}(r) \mathrm{d}r f_\theta(\theta) \mathrm{d}\theta. \quad (8)$$

Similarly, in the case of users in the cell edge area,

$$\bar{\rho}^{\mathrm{e}} = \mathbb{E}_z[\rho(\gamma(z), \Delta) | r \geq R_{\mathrm{c}}],$$
$$= \int_0^{2\pi} \int_{R_{\mathrm{c}}}^{R_{\mathrm{e}}} \rho(\gamma(r, \theta), \Delta) f_{r|r\geq R_{\mathrm{c}}}(r) \mathrm{d}r f_\theta(\theta) \mathrm{d}\theta. \quad (9)$$

In the case of FR scheme, we have $\Delta = 1$. By using (7), the corresponding average spectral efficiency can be calculated as:

$$\bar{\rho}_{\mathrm{FR}} = \mathbb{E}_z[\rho(\gamma_{\mathrm{FR}}(z), 1)]. \quad (10)$$

For comparison purpose, the cell edge user spectral efficiency in the case of FR scheme can be calculated as:

$$\bar{\rho}_{\mathrm{FR}}^{\mathrm{e}} = \mathbb{E}_z[\rho(\gamma_{\mathrm{FR}}(z), 1) | r \geq R_{\mathrm{c}}]. \quad (11)$$

B. Strict Fractional Frequency Reuse

1) SINR and Its Statistics: In a sFFR system, the SINR at z on a subcarrier in the common sub-band can be written as:

$$\gamma^{\mathrm{c}}(z) = \frac{(r^2 + h^2)^{-m-3}}{\sum_{i \in \mathcal{И}} (r_i^2(z) + h^2)^{-m-3} + \frac{1+2\delta^2}{3}\Omega}. \quad (12)$$

According to the frequency plan defined in II-D1, the SINR at z on a subcarrier in protected sub-bands $\gamma^{\mathrm{e}}(z)$ can also be calculated using (12) except for substituting $\mathcal{И}_{\mathrm{A}}$ for $\mathcal{И}$. The factor $\frac{1+2\delta^2}{3}$ of Ω is due to the change of the number of used subcarriers in sFFR compared to the case of the FR system. Since a fixed amount of available electrical power and an equal power distribution on each subcarrier are assumed, varying the number of used subcarriers causes change in the available power on each subcarrier.

When determining the distribution of SINR for a sFFR system, both cases of a user in the cell central area and a user in the cell edge area need to be considered. The overall CDF of the SINR can be calculated as follows:

$$\mathbb{P}[\gamma_{\mathrm{sFFR}} < T] = \mathbb{P}[r < R_{\mathrm{c}}]\mathbb{P}[\gamma^{\mathrm{c}} < T | r < R_{\mathrm{c}}]$$
$$+ \mathbb{P}[r \geq R_{\mathrm{c}}]\mathbb{P}[\gamma^{\mathrm{e}} < T | r \geq R_{\mathrm{c}}], \quad (13)$$

where $\mathbb{P}[\gamma^{\mathrm{c}} < T | r < R_{\mathrm{c}}]$ and $\mathbb{P}[\gamma^{\mathrm{e}} < T | r \geq R_{\mathrm{c}}]$ are the CDF of the SINR with the conditions that the user is in the cell centre using common sub-band and is in the cell edge using protected sub-band, respectively. They can be calculated using the same method as that described in Section III-A2.

2) Spectral Efficiency: Since the average spectral efficiency varies in different sub-bands, the overall average spectral efficiency should be the average over the whole frequency band. When there are users in both the cell central area and the cell edge area, the overall average spectral efficiency can be calculated as [28]:

$$\bar{\rho}_{\mathrm{sFFR,nor}} = \zeta^{\mathrm{c}}\bar{\rho}^{\mathrm{c}} + \zeta^{\mathrm{e}}\bar{\rho}^{\mathrm{e}},$$

where $\bar{\rho}^{\mathrm{c}}$ ($\bar{\rho}^{\mathrm{e}}$) is the average spectral efficiency for the users taking the common (protected) sub-band for transmission; ζ^{c} and ζ^{e} are the averaging weights for $\bar{\rho}^{\mathrm{c}}$ and $\bar{\rho}^{\mathrm{e}}$, respectively. The averaging weight ζ of an average spectral efficiency $\bar{\rho}$ is calculated as:

$$\zeta = \frac{\Delta K_{\bar{\rho}}}{\tilde{K}}, \quad (14)$$

where $K_{\bar{\rho}}$ refers to the number of subcarriers that achieve an average spectral efficiency of $\bar{\rho}$. All ζ for FFR can be simply derived according to the FFR schemes described in Section II-D. Since all of the averaging weights ζ follow the same rule as (14), and the derivations of each ζ is long but very simple, it would be unnecessary to list all of the derivations of all of the ζs. Only the final results are listed. In the case of sFFR here, ζ^{c} and ζ^{e} can be found as $\zeta^{\mathrm{c}} \cong \delta^2$ and $\zeta^{\mathrm{e}} \cong 1 - \delta^2$, respectively [28].

The cell centre users use the common sub-band with $\Delta = 1$, while the cell edge users use the protected sub-band with $\Delta = 3$. Therefore, in conjunction with (8) and (9), $\bar{\rho}^{\mathrm{c}}$ and $\bar{\rho}^{\mathrm{e}}$ in sFFR case can be calculated as:

$$\bar{\rho}^{\mathrm{c}} = \mathbb{E}_z[\rho(\gamma^{\mathrm{c}}(z), 1) | r < R_{\mathrm{c}}],$$
$$\bar{\rho}^{\mathrm{e}} = \mathbb{E}_z[\rho(\gamma^{\mathrm{e}}(z), 3) | r \geq R_{\mathrm{c}}]. \quad (15)$$

An optical attocell network is a small-cell cellular network in which each BS serves several users and these users are fewer than those in a normal RF cell. Consequently, the problem of an uneven load in different cells is more critical in an optical attocell network. In some extreme cases, there may be no user in a cell when the user density is very low. The use of the FFR technique makes this issue even worse. Since the cell coverage area is divided into centre and edge areas, which are smaller compared with the total cell coverage area, the chance that no active user is present in a specified region (a cell centre or a cell edge area) will be much higher. Consequently, in the case of no user present in a specified area, the corresponding assigned sub-band remains idle, which is a waste of transmission resources. Therefore, the case of no user present in the cell central or edge area needs to be considered. Since the common sub-band is restricted to the cell edge users, for the case that there is no user in the central area, the common sub-band is wasted and $\zeta^{\mathrm{c}} = 0$. Therefore, the corresponding average spectral efficiency is only $\zeta^{\mathrm{e}}\bar{\rho}^{\mathrm{e}}$. For the same reason, when there is no user present in the cell edge area, the average spectral efficiency is only $\zeta^{\mathrm{c}}\bar{\rho}^{\mathrm{c}}$. Thus, the final average spectral efficiency achieved by a sFFR system can be calculated as:

$$\bar{\rho}_{\mathrm{sFFR}} = \mathcal{P}_{\mathrm{c}}\zeta^{\mathrm{c}}\bar{\rho}^{\mathrm{c}} + \mathcal{P}_{\mathrm{e}}\zeta^{\mathrm{e}}\bar{\rho}^{\mathrm{e}}$$
$$+ (1 - \mathcal{P}_{\mathrm{c}} - \mathcal{P}_{\mathrm{e}})(\bar{\rho}_{\mathrm{sFFR,nor}}), \quad (16)$$

where $\mathcal{P}_{\mathrm{c}}$ ($\mathcal{P}_{\mathrm{e}}$) denotes the probability that all of the observed users fall into the cell centre (edge) area. It is assumed that the user spatial distribution follows a PPP with a user density of λ. By limiting the users in a specified area of A, the mean number of users within this area is $A\lambda$. According to the probability

mass function of the Possion distribution, the probability that no user in this area is given as:

$$\mathcal{P}_0 = e^{-A\lambda}.$$

The area of a cell can be found as $A_{\text{cell}} = \pi R_e^2$ according to the geometry shown in Fig. 7. Then, the cell central area and the cell edge area are $A_{\text{cell}}\delta^2$ and $A_{\text{cell}}(1 - \delta^2)$, respectively. Therefore, $\mathcal{P}_c$ and $\mathcal{P}_e$ can be calculated as:

$$\mathcal{P}_c = e^{-A_{\text{cell}}(1-\delta^2)\lambda},$$

$$\mathcal{P}_e = e^{-A_{\text{cell}}\delta^2\lambda}.$$

Since the cell edge users only use the protected sub-band for transmission, the cell edge spectral efficiency for sFFR can be calculated using (15).

C. Soft Frequency Reuse

1) SINR and Its Statistics: In a SFR system, due to the more complex SFR scheme, there are five conditions in the SFR system SINR calculation. In order to efficiently present these SINR expressions, a function is defined as follows:

$$\chi(p_0, p_1, p_2, p_3, z)$$
$$= \frac{p_0 (r^2 + h^2)^{-m-3}}{\Upsilon(p_1, p_2, p_3, z) + (\beta(1 - \max(\delta^2, \frac{2}{3})) + \delta^2)\Omega},$$

where p_0, p_1, p_2, p_2 are the power control factors which equals β or 1 or 0, and

$$\Upsilon(p_1, p_2, p_2, z) = p_1 \sum_{i \in \mathcal{H}_A} (r_i^2(z) + h^2)^{-m-3}$$
$$+ p_2 \sum_{i \in \mathcal{H}_B} (r_i^2(z) + h^2)^{-m-3} + p_3 \sum_{i \in \mathcal{H}_C} (r_i^2(z) + h^2)^{-m-3}.$$

According to the five cases shown in Fig. 8(b) and (c), the corresponding SINR in each cases can be calculated as follows: $\gamma_1^e(z) = \chi(\beta, \beta, 1, 1, z)$, $\gamma_2^e(z) = \chi(\beta, \beta, 0, 0, z)$, $\gamma_1^c(z) = \chi(1, 1, 1, 1, z)$, $\gamma_2^c(z) = \chi(1, 1, \beta, 1, z)$ and $\gamma_3^c(z) = \chi(1, 1, 1, \beta, z)$. According to the frequency plan described in Section II-D2 and (14), the corresponding averaging weights for average spectral efficiency with each γ are calculated as:

$$\zeta_1^e = \zeta_2^c = \zeta_3^c \cong \frac{2}{3} - \max\left(\delta^2, \frac{2}{3}\right) + \frac{1}{2}\min\left(\delta^2, \frac{2}{3}\right),$$

$$\zeta_2^e \cong 1 - \frac{3}{2}\min\left(\delta^2, \frac{2}{3}\right) \text{ and } \zeta_1^c \cong 3\max\left(\delta^2, \frac{2}{3}\right) - 2.$$

Similar to the case of sFFR, Ω is multiplied by a scaling factor to compensate for the change in transmission power on each subcarrier.

The SINR CDF of a SFR system can be calculated by:

$$\mathbb{P}[\gamma_{\text{SFR}} < T] = \mathbb{P}[r < R_c]\mathbb{P}[\gamma_{\text{SFR}} < T|r < R_c]$$
$$+ \mathbb{P}[r \geq R_c]\mathbb{P}[\gamma_{\text{SFR}} < T|r \geq R_c]. \quad (17)$$

According to the resource plan described in Section II-D2, it is noted that a user in a SFR system receives the signal on

multiple subcarriers with different SINR. To simplify the calculation, the SINR experienced by a user in a SFR system is defined as follows: the user randomly selects one of the available subcarriers for transmission, and the SINR experienced on the selected subcarrier is $\tilde{\gamma}$. In (17), the cell edge user SINR distribution $\mathbb{P}[\gamma_{\text{SFR}} < T|r \geq R_c]$ can be calculated as:

$$\mathbb{P}[\gamma_{\text{SFR}} < T|r \geq R_c] = \mathbb{P}[\tilde{\gamma} = \gamma_1^e]\mathbb{P}[\gamma_1^e < T|r \geq R_c]$$
$$+ \mathbb{P}[\tilde{\gamma} = \gamma_2^e]\mathbb{P}[\gamma_2^e < T|r \geq R_c],$$

where $\mathbb{P}[\tilde{\gamma} = \gamma]$ refers to the probability that the subcarrier with a SINR of γ is selected. $\mathbb{P}[\tilde{\gamma} = \gamma_1^e]$ and $\mathbb{P}[\tilde{\gamma} = \gamma_2^e]$ can be calculated as:

$$\mathbb{P}[\tilde{\gamma} = \gamma_1^e] = \frac{\zeta_1^e}{\zeta_1^e + \zeta_2^e/3} = \frac{3}{2}\min\left(\delta^2, \frac{2}{3}\right),$$

$$\mathbb{P}[\tilde{\gamma} = \gamma_2^e] = 1 - \mathbb{P}[\tilde{\gamma} = \gamma_1^e] = 1 - \frac{3}{2}\min\left(\delta^2, \frac{2}{3}\right).$$

Similarly, the centre user SINR CDF $\mathbb{P}[\gamma_{\text{SFR}} < T|r < R_c]$ can be calculated as:

$$\mathbb{P}[\gamma_{\text{SFR}} < T|r < R_c] = \mathbb{P}[\tilde{\gamma} = \gamma_1^c]\mathbb{P}[\gamma_1^c < T|r < R_c]$$
$$+ \mathbb{P}[\tilde{\gamma} = \gamma_2^c]\mathbb{P}[\gamma_2^c < T|r < R_c] + \mathbb{P}[\tilde{\gamma}$$
$$= \gamma_3^c]\mathbb{P}[\gamma_3^c < T|r < R_c],$$

where

$$\mathbb{P}[\tilde{\gamma} = \gamma_1^c] = \frac{\zeta_1^c}{\zeta_1^c + \zeta_2^c + \zeta_3^c} = 3 - \frac{2}{\max(\delta^2, \frac{2}{3})},$$

$$\mathbb{P}[\tilde{\gamma} = \gamma_2^c] = \mathbb{P}[\tilde{\gamma} = \gamma_3^c] = \frac{\zeta_2^c}{\zeta_1^c + \zeta_2^c + \zeta_3^c} = \frac{1}{\max(\delta^2, \frac{2}{3})} - 1.$$

All the conditional CDF of the SINR in each case can be calculated using the method described in Section III-A2.

2) Spectral Efficiency: When there are users in both the cell central and the cell edge areas, the overall average spectral efficiency of a SFR system can be determined as follows:

$$\bar{\rho}_{\text{SFR,nor}} = \zeta_1^e \bar{\rho}_1^e + \zeta_2^e \bar{\rho}_2^e + \zeta_1^c \bar{\rho}_1^c + \zeta_2^c \bar{\rho}_2^c + \zeta_3^c \bar{\rho}_3^c,$$

where $\bar{\rho}_1^e, \bar{\rho}_2^e, \bar{\rho}_1^c, \bar{\rho}_2^c$ and $\bar{\rho}_3^c$ denote the achievable average spectral efficiency corresponding to $\gamma_1^e, \gamma_2^e, \gamma_1^c, \gamma_2^c$ and γ_3^c, respectively. They can be calculated using (8) and (9) as:

$$\bar{\rho}_1^e = \mathbb{E}_z[\rho(\gamma_1^e(z), 1)|r \geq R_c],$$

$$\bar{\rho}_2^e = \mathbb{E}_z[\rho(\gamma_2^e(z), 3)|r \geq R_c],$$

$$\bar{\rho}_1^c = \mathbb{E}_z[\rho(\gamma_1^c(z), 1)|r < R_c],$$

$$\bar{\rho}_2^c = \mathbb{E}_z[\rho(\gamma_2^c(z), 1)|r < R_c],$$

$$\bar{\rho}_3^c = \mathbb{E}_z[\rho(\gamma_3^c(z), 1)|r < R_c].$$

Similar to the sFFR case, the problem of no user in a specified area needs to be considered. Accounting for no user in the cell edge and also the cell central area, the final average spectral efficiency of a SFR system can be found:

$$\bar{\rho}_{\text{SFR}} = \mathcal{P}_c(\zeta_1^c \bar{\rho}_1^c + \zeta_2^c \bar{\rho}_2^c + \zeta_3^c \bar{\rho}_3^c) + \mathcal{P}_e(\zeta_1^e \bar{\rho}_1^e + \zeta_2^e \bar{\rho}_2^e)$$
$$+ (1 - \mathcal{P}_c - \mathcal{P}_e)\bar{\rho}_{\text{SFR,nor}}. \quad (18)$$

TABLE II
SYSTEM PARAMETERS

Parameter	Symbol	Value
LED half-power semi-angle	$\phi_{1/2}$	$60°$
Vertical separation	h	2.15 m
PD area	A_{pd}	1 cm^2
Modulation bandwidth	W	40 MHz
PD responsivity	R_{pd}	0.1 A/W
DC bias factor	κ	3

TABLE III
BS OUTPUT OPTICAL POWER CONFIGURATION

cell radius R [m]	BS output optical power P_{opt} [W]	average illuminance $\bar{E}_v$ [lx]	illuminance uniformity U_0
2	24	519	0.84
2.25	29	513	0.83
2.5	35	509	0.81
2.75	41	507	0.77
3	48	506	0.73
3.25	56	505	0.69

The cell edge spectral efficiency in a SFR system can be calculated as:

$$\bar{\rho}^e_{\text{SFR}} = \frac{K_{\bar{\rho}^e_1}}{K_e}\bar{\rho}^e_1 + \frac{3K_{\bar{\rho}^e_2}}{K_e}\bar{\rho}^e_2 = \frac{\zeta^e_1\bar{\rho}^e_1 + \zeta^e_2\bar{\rho}^e_2}{1-\delta^2}. \quad (19)$$

IV. RESULTS AND PERFORMANCE ANALYSIS

In this section, the performance of the considered FFR schemes in an optical attocell network in terms of SINR CDF, average spectral efficiency and cell edge spectral efficiency are evaluated. Interference mitigation and improvement in cell edge and average spectral efficiency are expected by using FFR schemes.

A. Parameter Configurations

The system parameters of the evaluated systems are listed in Table II. These values are the default settings in the results presented in this section if the parameters are not otherwise specified. A $\phi_{1/2}$ of $60°$ is reasonable for lighting performance. A vertical separation between a BS and a user h of 2.15 m is considered due to a user equipment height of 0.85 m and a ceiling height of 3 m. A PD physical area A_{pd} of 1 cm^2 is the generally acceptable in VLC systems [3], [29]. The 40 MHz modulation bandwidth agrees with the 20 MHz flat bandwidth that is provided by a phosphorescent white light LED with equalisation [30]. A PD responsivity R_{pd} of 0.1 is suitable when the receiver only accepts the blue component of light [3]. Since only the negative samples of the OFDM signal after adding the dc-bias is clipped, the dc-bias level κ is equivalent to the bottom clipping level; κ is set to 3, since this value is sufficient to minimise the clipping noise to a level that causes negligible distortion in the transmission [31].

A single LED chip with a typical low rated output optical power cannot provide sufficient optical power to meet the standard lighting requirements. Therefore, multiple LED chips are integrated within an LED luminary, which provide much higher power than a single chip. To simplify the radiation model, each LED light luminary is treated as a point source. In this study, the configuration of the BS output power takes the illumination requirement into account. An average illuminance of at least 500 lx and an illuminance uniformity of at least 0.6 is required in an room used for writing or reading purposes [32]. In this study, the required optical output power that fulfils the illuminance requirement is found to be highly related to the cell radius R. Therefore, the BS output optical power P_{opt} is configured
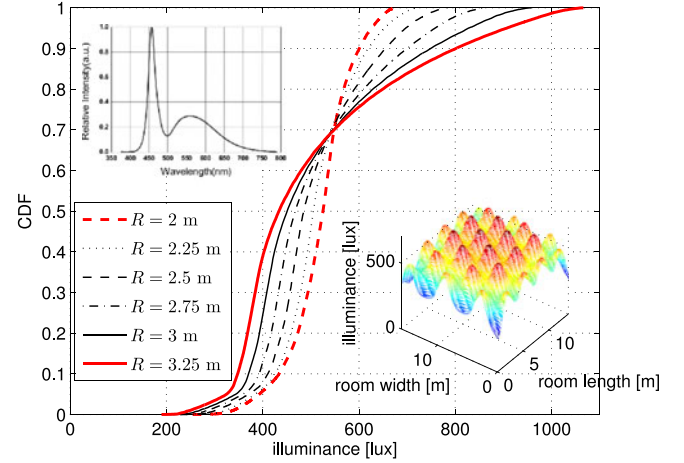

Fig. 9. Illuminance distribution in a room with 27 cells. The network deployment is the same as that shown in Fig. 2, except for the difference in cell radius. The illuminance spatial distribution with $R = 2$ m is shown in the sub-figure on the bottom right. The relative intensity of the LED output against wavelength is shown in the sub-figure on the top left, which is used for the calculation of illuminance.

based on the value of R. The considered configuration in this study is listed in Table III. The corresponding illuminance distribution in a room with 27 cells (the cell deployment is shown in Fig. 2) in the form of CDF is presented in Fig. 9. The notable illumination results are summarised in Table III.

B. SINR Statistics Results

Fig. 10 shows the results of the SINR statistics based on the two-layer hexagonal network model. Here the noise level is $N_0 = 1 \times 10^{-21}$ A^2/Hz and cell radius is $R = 2.5$ m. In the FFR systems, $\delta = 0.7$ and $\beta = 2$. These results include the calculation using (6), (13) and (17) in the analysis presented in Section III using the numerical method, and the corresponding empirical statistics obtained by Monte Carlo simulation. The agreement between the two results validate the analysis. In addition, the simulation of the deployed networks are presented to validate the accuracy of the estimation by using two-layer network model. As expected, there is an acceptable difference, less than 2 dB, between the results of two-layer network model and those of the deployed network with only 12 cells (room size 10.8 m $\times$ 12.5 m) due to the room edge effects. However, with an increase of the number of cells, the difference between the curves of the case with deployed network and that for the
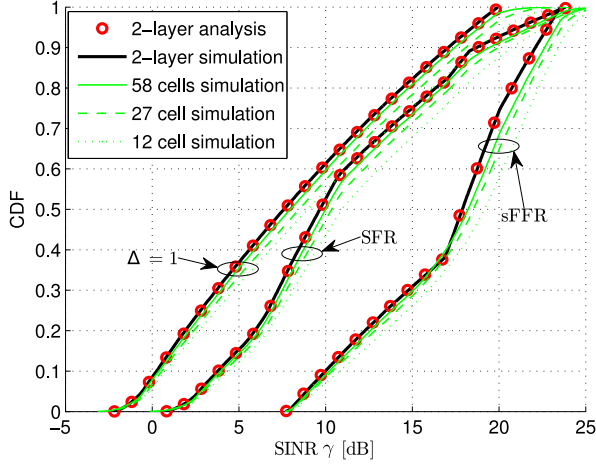
Fig. 10. SINR statistics for different reuse schemes. The network deployment in the room with 12 and 27 cells are the same as those shown in Fig. 5, except for the difference in cell radius. System parameters: $N_0 = 1 \times 10^{-21}$ A^2/Hz, $R = 2.5$ m, $\delta = 0.7$ and $\beta = 2$.

Fig. 11. Average spectral efficiency and cell edge spectral efficiency against cell radius R. System parameters: $\delta = 0.7$, $N_0 = 1 \times 10^{-21}$ A^2/Hz and $\lambda = 1$ user/m^2.

Fig. 12. Average spectral efficiency against δ. System parameters: $R = 2.5$ m, $\lambda = 1$ user/m^2 and $\beta = 2$.

two-layer network diminishes. In the case of 58 cells (room size 26 m × 30 m), the SINR CDF differences decrease to be in a range between 0.3 to 0.7 dB. Note that another source of mismatch is the circular cell approximation of the 0th cell in the two-layer network model. This mismatch is considered reasonable in many cellular system analysis [28]. Therefore, the performance of the two-layer network model is a reasonable estimation to the practical optical attocell system.

As shown in Fig. 10, the FR system exhibits the worst SINR as expected. In contrast, FFR schemes offer an improved SINR. The sFFR system and the SFR system show improvements of 9.74 and 3.54 dB in terms of minimum SINR (at 10th percentile), respectively. In addition, they also show improvements of 10.3 and 2.07 dB in terms of medium SINR, respectively. Note that the bends in the FFR curves are the results of combining different SINR statistics in multiple regions in a cell and in different sub-bands. These combinations can be observed in the analysis in Sections III-B1 and III-C1.

C. Spectral Efficiency Results

In this section, average spectral efficiency, calculated using (10), (16) and (18), is the metric to demonstrate the improvement in the overall system capacity. In addition, average spectral efficiency in the cell edge area, calculated using (11), (15) and (19), is the metric to show the improvement in cell edge user experience.

1) Effect of Cell Radius: Fig. 11 shows the average spectral efficiency and the cell edge spectral efficiency results with different cell radius R. In these results, $\delta = 0.7$, $N_0 = 1 \times 10^{-21}$ A^2/Hz, and $\lambda = 1$ user/m^2. Both the analytical calculation and the simulation are presented. The close agreement validates the related analysis. With a fixed $\phi_{1/2}$, the increase of cell radius results in a decrease in the interference between users in adjacent cells [27]. In other words, a larger cell provides better overall signal quality. In addition, a smaller cell leads to a higher value of $\mathcal{P}_c$ and $\mathcal{P}_e$, which results in loss in average
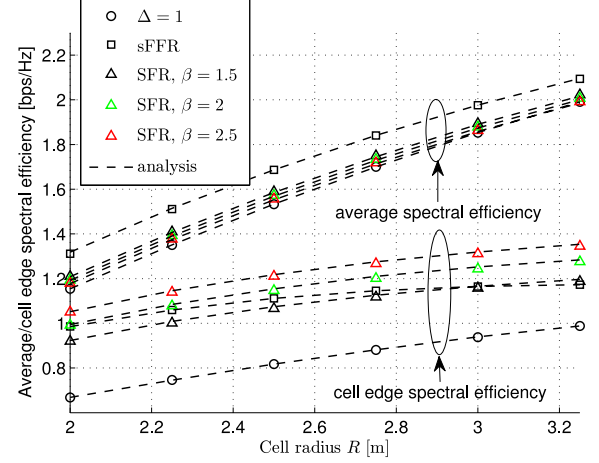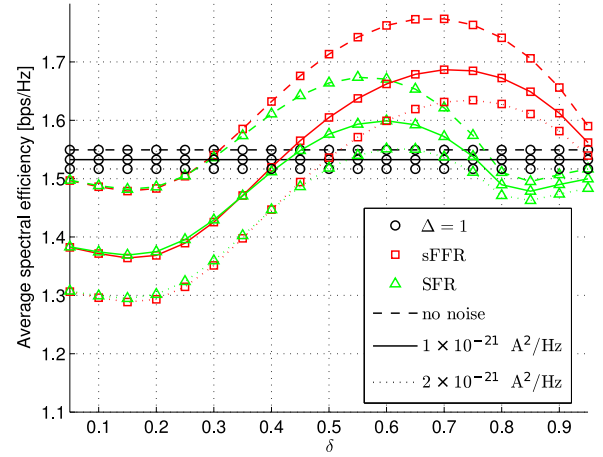
spectral efficiency in FFR systems. Therefore, both the average spectral efficiency and the cell edge spectral efficiency for any reuse scheme is an increasing function of R.

The improvement of using sFFR is in the range from 5% to 14% in terms of average spectral efficiency and is in the range from 19% to 47% in terms of cell edge spectral efficiency. The improvement of using SFR is in the range from 0% to 5% in terms of average spectral efficiency and is in the range from 21% to 57% in terms of cell edge spectral efficiency. Generally, the sFFR system achieves the highest average spectral efficiency. The SFR system is more flexible, since it can achieve a good balance between cell edge user performance and overall system performance by adjusting parameter β. Both sFFR and SFR schemes improved the cell edge user experience significantly.

2) Effects of δ and Noise Level: Fig. 12 shows the average spectral efficiency against δ. In the results, $R = 2.5$ m, $\lambda = 1$ user/m^2 and $\beta = 2$ in SFR systems. As shown in Section II-D, the channel assignment is proportional to the corresponding coverage area for FFR systems. When δ is too small, the majority of the users are cell edge users who are assigned a reuse factor
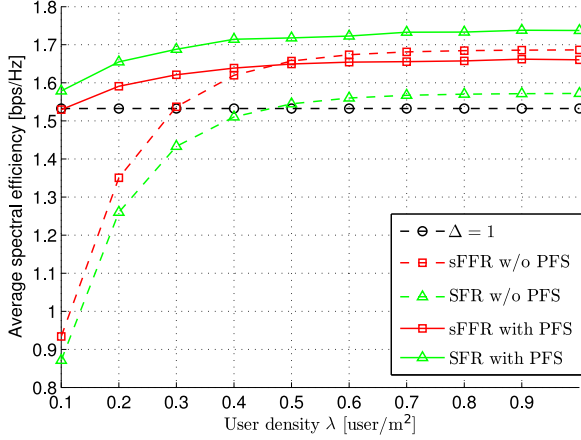
Fig. 13. Average spectral efficiency against user density λ. System parameters: $\delta = 0.7$, $R = 2.5$ m, $N_0 = 1 \times 10^{-21}$ A^2/Hz and $\beta = 2$.

of 3, which considerably decreases the spectral efficiency of the system. When δ is too large, fewer users can be covered by the cell edge area. Consequently, average spectral efficiency decreases significantly due to the increased interference received by the cell centre users who are close to the edge of the cell central area ($r \to R_c$). In addition, when δ is close to 0 or 1, either $\mathcal{P}_c$ or $\mathcal{P}_e$ is significant, which also causes a decrease in spectral efficiency.

Fig. 12 also shows the cases with different noise levels. Intuitively, the higher the noise level, the lower the average spectral efficiency for systems with any reuse schemes. In addition, the higher the noise level, the lower improvement that can be obtained from the FFR schemes. For example, when considering the improvement of the sFFR scheme with optimal δ, the improvement in terms of average spectral efficiency is 15% if there is no receiver noise. However, this improvement decreases to 8% if the noise level is increased to $N_0 = 2 \times 10^{-21}$ A^2/Hz. Furthermore, it is noted that the noise level may affect the optimal configuration of δ. When noise is not considered, the optimal δ for sFFR is around 0.7 and this is in line with [28]. In the case of SFR, the optimal δ is around 0.55. However, with the increase in the noise level, optimal δs for FFR systems increase to a slightly higher level.

3) Effects of Active User Density and Proportional Fairness Scheduling (PFS): As shown in Section III-B2, the user density λ is crucial to the value of $\mathcal{P}_c$ and $\mathcal{P}_e$, which may cause a significant effect on the system spectral efficiency. Fig. 13 shows the effect of user density on the average spectral efficiency of different systems. In the results, $\delta = 0.7$, $R = 2.5$ m, $N_0 = 1 \times 10^{-21}$ A^2/Hz and $\beta = 2$ in SFR systems. Both FFR systems show a similar trend with respect to the variations in the λ. Generally, if λ is too small, the average spectral efficiency of FFR systems decreases significantly. For example, in the case of $\lambda = 0.1$ user/m^2, the FFR system exhibits an average spectral efficiency lower than 1 bps/Hz, which is much lower than the benchmark.

In order to solve the issue caused by low user density, PFS [33] is considered in conjunction with the FFR techniques.

With a given FR scheme, there are L different sub-bands for transmission. The sub-band l has K_l subcarriers, where $l = 1, 2, \cdots, L$. $K_{l,n}$ subcarriers in sub-band l are assigned to user n. Thus $\sum_{n=1}^{N} K_{l,n} = K_l$. Therefore, the data rate achieved by user n can be calculated as follows:

$$C_n = \sum_{l=1}^{L} K_{l,n} s_{l,n},$$

where $s_{l,n}$ is the achievable data rate by user n on a subcarrier in sub-band l. With a given system realisation, user locations are determined. Therefore, all $s_{l,n}$ are fixed for that realisation. In this study, PFS aims at maximising the following objective function:

$$\Lambda = \sum_{n=1}^{N} \ln\left(C_n\right). \tag{20}$$

Conventional per subcarrier PFS requires channel frequency selectivity to converge to a robust solution. However, the assumptions used in this study make the channel gain flat within each sub-band. This causes problems in the convergence of the scheduling solution by using the per subcarrier based PFS. Therefore, an alternative algorithm is used to achieve the same PFS function. The details of this modified PFS is introduced as follows. A scheduling plan matrix is defined as:

$$\mathbf{K} = \begin{bmatrix} K_{1,1} & \cdots & K_{L,1} \\ \vdots & \ddots & \vdots \\ K_{1,N} & \cdots & K_{L,N} \end{bmatrix},$$

which lists the $K_{l,n}$ for all users in every sub-bands. Based on a specified $\mathbf{K}$, the corresponding set of user data rates can be calculated as follows:

$$\mathbf{C}\{\mathbf{K}\} = \begin{bmatrix} C_1\left(K_{1,1} & \cdots & K_{L,1}\right) \\ \vdots \\ C_N\left(K_{1,N} & \cdots & K_{L,N}\right) \end{bmatrix}.$$

The modified PFS algorithm is listed in Algorithm 1. The α in Algorithm 1 is a forgetting factor for the calculation of average user data rate $\bar{\mathbf{C}}$. The proof of Algorithm 1 maximising (20) is shown in Appendix B.

PFS can achieve a good balance between spectral efficiency and user fairness. More importantly, it can dynamically distribute spectral resources depending on the current load condition. With this benefit of PFS, the sub-band availability constraint can be adjusted as follows: the whole sub-band assigned to a cell is available to any active user in that cell. In the case of no user in the cell edge (centre) area of the cell, PFS will assign the resources preserved for edge (centre) users to centre (edge) users. Note that although cell edge users achieve low SINR by using the sub-band prepared for centre users, through appropriate modulation and coding adjustment, transmission with low spectral efficiency can be established [34], which is better than the sub-band being unused. This is the reason for the PFS

approach improving the FFR system performance when user density is low. Under conditions where users are present in both areas, PFS avoids assigning subcarriers in sub-bands for centre user to edge users, because these resources are extremely inefficient for cell edge users. Consequently, the majority of the transmission resources are assigned to the cell centre users. Since PFS has the ability to keep the fairness between centre and edge user, it will prevent the centre users accessing 'good' resources in the protected sub-band. Therefore, PFS also avoids assigning subcarriers in sub-bands for cell edge users to centre users. This is the reason why the sub-band availability constraint can be lessened when PFS is used in FFR systems. Additionally, due to the small number of users in an optical attocell, the computational complexity of the PFS will be much lower than the PFS in conventional RF cellular systems.

In Fig. 13, the average spectral efficiency of the FFR systems with PFS are also demonstrated. It can be observed that PFS effectively alleviates the spectral efficiency decrease for FFR systems under the condition of low λ. In addition, it is noted that the performance of sFFR with PFS and $\lambda = 1$ user/m^2 is slightly worse compared with that without PFS. This is because the data rate difference between centre users and edge users is significant. Therefore, the PFS trades some spectral efficiency for better fairness. In the case of SFR with $\lambda = 1$ user/m^2, PFS further increases the average spectral efficiency. This is because the data rate gap between centre users and edge users is small. Therefore, the PFS can gain additional spectral efficiency with a low loss of fairness.

V. Conclusion

A DCO-OFDM-based optical attocell network with FFR schemes was considered in this paper. An analytical framework of the FFR application in an optical attocell network was proposed. Both the sFFR and SFR schemes were considered. A method of calculating the statistics of the achievable SINR and the average spectral efficiency in a two-layer network model was presented. The numerical results show a close agreement with the results of the Monte Carlo simulations. By comparing with the networks deployed in a rectangular room, the performance of the two-layer model was demonstrated to be a good estimation of the practical optical attocell network. The performance of the optical attocell network with FFR was evaluated and compared with a benchmark system with full frequency reuse scheme. The results showed that FFR schemes can effectively improve the downlink SINR in an optical attocell network. In addition, FFR schemes offer significant improvements in the cell edge spectral efficiency of an optical attocell system. Furthermore, the average spectral efficiency is slightly improved. Also, the effects of the key parameters were studied, such as cell radius R, cell centre/radius ratio δ and active use density λ. It was identified that the optimal value for δ is 0.7 for sFFR and 0.55 for SFR. With an increase in the noise level, these optimal values become greater and the gain from FFR schemes decreases. In addition, a low user density λ significantly decreases the achievable average spectral efficiency. However, PFS can be used to effectively alleviate this problem.

Algorithm 1 : Proportional fairness scheduling

1: **for** $l = 1, 2, \ldots, L$ **do**
2: $\quad K_{l,1} = K_{l,2} = \cdots = K_{l,N} = K_l/N$
3: **end for**
4: $\bar{\mathbf{C}} = \mathbf{C}\{\mathbf{K}\}$
5: **for** $l = 1, 2, \ldots, L$ **do**
6: $\quad \mathbf{S} = \left[\frac{s_{l,1}}{\bar{\mathbf{C}}_1}, \frac{s_{l,2}}{\bar{\mathbf{C}}_2}, \ldots, \frac{s_{l,N}}{\bar{\mathbf{C}}_N} \right]$ and $\mathbf{S}_n = \frac{s_{l,n}}{\bar{\mathbf{C}}_n}$.
7: $\quad n_{\max} = \arg\max_n \mathbf{S}_n$ and $n_{\min} = \arg\min_n \mathbf{S}_n$.
8: $\quad$ **if** $K_{l,n_{\max}} < K_l$ **then**
9: $\quad\quad$ **if** $K_{l,n_{\min}} = 0$ **then**
10: $\quad\quad\quad$ Exclude $\mathbf{S}_{n_{\min}}$ from $\mathbf{S}$ and go back to step 8.
11: $\quad\quad$ **end if**
12: $\quad\quad K_{l,n_{\max}} = K_{l,n_{\max}} + 1, K_{l,n_{\min}} = K_{l,n_{\min}} - 1$
13: $\quad$ **end if**
14: **end for**
15: $\bar{\mathbf{C}} = \bar{\mathbf{C}}(1 - \alpha) + \mathbf{C}\{\mathbf{K}\}\alpha$
16: Iterate from step 6 to step 16 until $\mathbf{K}$ converge.

Appendix

A. SINR Simplification: $\Delta = 1$

In VLC systems, the limiting factor of the LED transmitter is its average optical power output. Therefore, it is reasonable to calculate the maximum acceptable signal electrical power based on the available optical power output of the LED transmitter. In [35], it is shown in DCO-OFDM that:

$$\frac{P_{\mathrm{opt}}^2}{P_{\mathrm{elec,AC}} + x_{\mathrm{DC}}^2} = \frac{\kappa^2}{1 + \kappa^2},$$

where P_{opt} is the average optical output of the LED transmitter and κ is a parameter reflecting the dc-bias level which is given as $\kappa = x_{\mathrm{DC}}/\sqrt{P_{\mathrm{elec,AC}}}$. Then we can find that $P_{\mathrm{elec,AC}} = P_{\mathrm{opt}}^2/\kappa^2$ and

$$P_{\mathrm{elec},i,k} = \frac{P_{\mathrm{opt}}^2}{(K-2)\kappa^2}. \tag{A.1}$$

Insert (A.1) and (1) in (3), it can be found that:

$$\gamma_{\mathrm{FR}}(z) = \frac{\frac{P_{\mathrm{opt}}^2 (m+1)^2 A_{\mathrm{pd}}^2 R_{\mathrm{pd}}^2 h^{2m+2} \left(r_0^2(z) + h^2 \right)^{-m-3}}{(2\pi)^2 (K-2)\kappa^2}}{\sum_{i \in \mathcal{U}} \frac{P_{\mathrm{opt}}^2 (m+1)^2 A_{\mathrm{pd}}^2 R_{\mathrm{pd}}^2 h^{2m+2} \left(r_i^2(z) + h^2 \right)^{-m-3}}{(2\pi)^2 (K-2)\kappa^2} + \sigma_k^2},$$

$$= \frac{\left(r^2 + h^2 \right)^{-m-3}}{\sum_{i \in \mathcal{U}} \left(r_i^2(z) + h^2 \right)^{-m-3} + \Omega},$$

where

$$\Omega = \frac{4\pi^2 (K-2) N_0 W \kappa^2}{K P_{\mathrm{opt}}^2 (m+1)^2 A_{\mathrm{pd}}^2 R_{\mathrm{pd}}^2 h^{2m+2}}.$$

B. Proportional Fairness Scheduling

In step 12 of Algorithm 1, $K_{l,n_{\max}}$ and $K_{l,n_{\min}}$ are adjusted while other elements in $\mathbf{K}$ remain the same. In this proof, we

only consider varying one of the L sub-bands $\hat{l}$. The resource allocation plan for other sub-bands remains the same. Since $\sum_n K_{\hat{l},n} = K_{\hat{l}}$, $K_{\hat{l},n_{\min}}$ varies if $K_{\hat{l},n_{\max}}$ changes its value. Their relationship is shown as follows:

$$K_{\hat{l},n_{\min}} = M - K_{\hat{l},n_{\max}},$$
$$M = K_{\hat{l}} - \sum_{n \neq n_{\min}, n_{\max}} K_{\hat{l},n}.$$

A variable $\hat{K}$ is defined to replace $K_{\hat{l},n_{\max}}$. Then Λ can be considered to be the function of $\hat{K}$. Thus, we can write Λ as:

$$\Lambda\left(\hat{K}\right) = \ln\left(C_{n_{\max}}\left(\hat{K}\right)\right)$$
$$+ \ln\left(C_{n_{\min}}\left(\hat{K}\right)\right) + \sum_{n \neq n_{\min}, n_{\max}} \ln\left(C_n\right)$$
$$= \ln\left(\hat{K} s_{\hat{l},n_{\max}} + \sum_{l \neq \hat{l}} K_{l,n_{\max}} s_{l,n_{\max}}\right)$$
$$+ \ln\left(\left(M - \hat{K}\right) s_{\hat{l},n_{\min}} + \sum_{l \neq \hat{l}} K_{l,n_{\min}} s_{l,n_{\min}}\right)$$
$$+ \sum_{n \neq n_{\min}, n_{\max}} \ln\left(C_n\right).$$

Then it can be found that:

$$\frac{d\Lambda\left(\hat{K}\right)}{d\hat{K}} = \frac{s_{\hat{l},n_{\max}}}{C_{n_{\max}}\left(\hat{K}\right)} - \frac{s_{\hat{l},n_{\min}}}{C_{n_{\min}}\left(\hat{K}\right)}.$$

If we let $\hat{K} = K_{\hat{l},n_{\max}}$, according to step 7 of Algorithm 1, we have that $\frac{d\Lambda(\hat{K})}{d\hat{K}} \geq 0$. This means that $\Lambda(\hat{K})$ is an increasing function at $K_{\hat{l},n_{\max}}$. Therefore, if we slightly increase $\hat{K}$, the probability that $\Lambda(\hat{K})$ will increase is high. To guarantee the convergence of Algorithm 1, the increment of $\hat{K}$ is minimised to one, since the number of subcarriers has to be an integer. With the updating of $\mathbf{K}$ in Algorithm 1, the values of elements in $\mathbf{S}$ in step 6 of Algorithm 1 will converge to a same value. When $\mathbf{S}$ converge for all sub-bands, Λ is maximised.

REFERENCES

[1] Visible light communication (VLC)—A potential solution to the global wireless spectrum shortage. (2011). GBI Research, Tech. Rep. GBISC017MR. [Online]. Available: http://www.gbiresearch.com/

[2] D. O'Brien, "Visible light communications: Challenges and potential," in *Proc. IEEE Photon. Conf.*, Arlington, VA, USA, Oct. 2011, pp. 365–366.

[3] L. Zeng, D. O'Brien, H. Minh, G. Faulkner, K. Lee, D. Jung, Y. Oh, and E. T. Won, "High data rate multiple input multiple output (MIMO) optical wireless communications using white LED lighting," *IEEE J. Sel. Areas Commun.*, vol. 27, no. 9, pp. 1654–1662, Dec. 2009.

[4] R. Mesleh, H. Elgala, and H. Haas, "Optical spatial modulation," *IEEE/OSA J. Opt. Commun. Netw.*, vol. 3, no. 3, pp. 234–244, Mar. 2011.

[5] J. Armstrong, "OFDM for optical communications," *J. Lightw. Technol.*, vol. 27, no. 3, pp. 189–204, Feb. 2009.

[6] D. Tsonev, S. Sinanovic, and H. Haas, "Complete modeling of nonlinear distortion in OFDM-based optical wireless communication," *J. Lightw. Technol.*, vol. 31, no. 18, pp. 3064–3076, Sep. 15, 2013.

[7] M. Alouini and A. Goldsmith, "Area spectral efficiency of cellular mobile radio systems," *IEEE Trans. Veh. Technol.*, vol. 48, no. 4, pp. 1047–1066, Jul. 1999.

[8] H. Haas, "High-speed wireless networking using visible light," *SPIE Newsroom*, Apr. 19, 2013, doi:10.1117/2.1201304.004773.

[9] D. Tsonev, H. Chun, S. Rajbhandari, J. J. D. McKendry, S. Videv, E. Gu, M. Haji, S. Watson, A. E. Kelly, G. Faulkner, M. D. Dawson, H. Haas, and D. O'Brien, "A 3-Gb/s single-LED OFDM-based wireless VLC link using a gallium nitride μLED," *IEEE Photon. Technol. Lett.*, vol. 26, no. 7, pp. 637–640, Apr. 2014.

[10] J. Fakidis, D. Tsonev, and H. Haas, "A comparison between DCO-OFDMA and synchronous one-dimensional OCDMA for optical wireless communications," in *Proc. IEEE 24th Int. Symp. Pers. Indoor Mobile Radio Commun.*, London, U.K., Sep. 8–11, 2013, pp. 3605–3609.

[11] G. W. Marsh and J. M. Kahn, "Channel reuse strategies for indoor infrared wireless communications," *IEEE Trans. Commun.*, vol. 45, no. 10, pp. 1280–1290, Oct. 1997.

[12] K. Cui, J. Quan, and Z. Xu, "Performance of indoor optical femtocell by visible light communication," *Opt. Commun.*, vols. 298/299, pp. 59–66, Jul. 2013.

[13] B. Ghimire and H. Haas, "Self-organising interference coordination in optical wireless networks," *EURASIP J. Wireless Commun. Netw.*, vol. 1, no. 131, Apr. 2012.

[14] T. Novlan, R. Ganti, A. Ghosh, and J. Andrews, "Analytical evaluation of fractional frequency reuse for OFDMA cellular networks," *IEEE Trans. Wireless Commun.*, vol. 10, no. 12, pp. 4294–4305, Dec. 2011.

[15] T. Novlan, J. Andrews, I. Sohn, R. Ganti, and A. Ghosh, "Comparison of fractional frequency reuse approaches in the OFDMA cellular downlink," in *Proc. IEEE Global Telecommun. Conf.*, Miami, FL, USA, Dec. 6–10, 2010, pp. 1–5.

[16] V. V. Huynh, N.-T. Le, N. Saha, M. Chowdhury, and Y. M. Jang, "Intercell interference mitigation using soft frequency reuse with two FOVs in visible light communication," in *Proc. Int. Conf. ICT Convergence*, Jeju Island, Korea, Oct. 15–17, 2012, pp. 141–144.

[17] C. Chen, N. Serafimovski, and H. Haas, "Fractional frequency reuse in optical wireless cellular networks," in *Proc. IEEE 24th Int. Symp. Pers. Indoor Mobile Radio Commun.*, London, U.K., Sep. 8–11, 2013, pp. 3594–3598.

[18] J. M. Kahn and J. R. Barry, "Wireless infrared communications," *Proc. IEEE*, vol. 85, no. 2, pp. 265–298, Feb. 1997.

[19] J. Barry, J. Kahn, W. Krause, E. Lee, and D. Messerschmitt, "Simulation of multipath impulse response for indoor wireless optical channels," *J. Sel. Areas Commun.*, vol. 11, no. 3, pp. 367–379, Apr. 1993.

[20] A. Goldsmith, *Wireless Communications*. Cambridge, U.K.: Cambridge Univ. Press, 2005.

[21] G. Cossu, A. M. Khalid, P. Choudhury, R. Corsini, and E. Ciaramella, "3.4 Gbit/s visible optical wireless transmission based on RGB LED," *Opt. Express*, vol. 20, pp. B501–B506, 2012.

[22] A. M. Khalid, G. Cossu, R. Corsini, P. Choudhury, and E. Ciaramella, "1-Gb/s transmission over a phosphorescent white LED by using rate-adaptive discrete multitone modulation," *IEEE Photon. J.*, vol. 4, no. 5, pp. 1465–1473, Oct. 2012.

[23] V. Jungnickel, V. Pohl, S. Nonnig, and C. von Helmolt, "A physical model of the wireless infrared communication channel," *IEEE J. Sel. Areas Commun.*, vol. 20, no. 3, pp. 631–640, Apr. 2002.

[24] H. Rohling, Ed., *OFDM: Concepts for Future Communication Systems*, 1st ed. Berlin, Germany: Springer-Verlag, 2011.

[25] S. Dimitrov, S. Sinanovic, and H. Haas, "Clipping noise in OFDM-based optical wireless communication systems," *IEEE Trans. Commun.*, vol. 60, no. 4, pp. 1072–1081, Apr. 2012.

[26] H. Elgala, R. Mesleh, and H. Haas, "Non-linearity effects and predistortion in optical OFDM wireless transmission using LEDs," *Int. J. Ultra Wideband Commun. Syst.*, vol. 1, no. 2, pp. 143–150, 2009.

[27] C. Chen, I. Muhammad, D. Tsonev, and H. Haas, "Analysis of downlink transmission in DCO-OFDM-based optical attocell networks," presented at the IEEE Global Telecommun. Conf., Austin, TX, USA, Dec. 8–12, 2014.

[28] H. Zhu and J. Wang, "Performance analysis of chunk-based resource allocation in multi-cell OFDMA systems," *IEEE J. Sel. Areas Commun.*, vol. 32, no. 2, pp. 367–375, Feb. 2014.

[29] T. Komine and M. Nakagawa, "Fundamental analysis for visible-light communication system using LED lights," *IEEE Trans. Consum. Electron.*, vol. 50, no. 1, pp. 100–107, Feb. 2004.

[30] J. Grubor, S. C. J. Lee, K.-D. Langer, T. Koonen, and J. W. Walewski, "Wireless high-speed data transmission with phosphorescent white-light

leds," in *Proc. 33rd Eur. Conf. Exhib. Opt. Commun.*, Berlin, Germany, Sep. 16–20, 2007.

[31] S. Dimitrov, H. Haas, M. Cappitelli, and M. Olbert, "On the throughput of an OFDM-based cellular optical wireless system for an aircraft cabin," in *Proc. Eur. Conf. Antennas Propag.*, Rome, Italy, Apr. 11–15, 2011, pp. 3089–3093.

[32] *Light and Lighting—Lighting of Work Places—Part 1: Indoor Work Places*, European Standard EN 12464-1, Jun. 2011.

[33] T.-D. Nguyen and Y. Han, "A proportional fairness algorithm with QoS provision in downlink OFDMA systems," *IEEE Commun. Lett.*, vol. 10, no. 11, pp. 760–762, Nov. 2006.

[34] H. Burchardt, Z. Bharucha, H. Haas, and G. Auer, "Uplink interference protection and fair scheduling for power efficient OFDMA networks," presented at the 8th Int. Workshop Multi-Carrier Systems Solutions, Herrsching, Germany, May 3–4, 2011.

[35] J. Armstrong and B. J. C. Schmidt, "Comparison of asymmetrically clipped optical OFDM and DC-biased optical OFDM in AWGN," *IEEE Commun. Lett.*, vol. 12, no. 5, pp. 343–345, May 2008.

Cheng Chen (S'14) received the B.Eng. degree in electronic and electrical engineering from the University of Strathclyde, Glasgow, U.K., in 2011, and the M.Sc. degree in communications and signal processing from the Imperial College London, London, U.K., in 2012. He is currently working toward the Ph.D. degree in electrical engineering at the University of Edinburgh, Edinburgh, U.K. His research interests include visible light communication networking and interference mitigation.

Stefan Videv received the B.Sc. degree in electrical engineering and computer science and the M.Sc. degree in communications, systems, and electronics from Jacobs University Bremen, Bremen, Germany, in 2007 and 2009, respectively, and the Ph.D. degree thesis titled techniques for green radio cellular communications from the University of Edinburgh, Edinburgh, U.K., in 2013. He is currently an Experimental Officer at the Li-Fi Research and Development Centre, University of Edinburgh, and is working in the field of visible light communications. His research interests include the prototyping of communication systems, smart resource allocation, and energy efficient communications.

Dobroslav Tsonev (S'11–M'14) received the B.Sc. degree in electrical engineering and computer science from Jacobs University Bremen, Bremen, Germany, in 2008, the M.Sc. degree in communication engineering with specialization in electronics from the Munich Institute of Technology, Munich, Germany, in 2010, and the Ph.D. degree in electrical engineering from the University of Edinburgh, Edinburgh, U.K., in 2015. He is currently a Research Associate at the Li-Fi Research and Development Centre, University of Edinburgh. His main research interests include optical wireless communications with an emphasis on visible light communications.

Harald Haas (S'98–AM'00–M'03) received the Ph.D. degree from the University of Edinburgh, Edinburgh, U.K., in 2001. He is currently the Chair of Mobile Communications at the University of Edinburgh. He was an invited speaker at TED Global 2011, and his talk has been watched online more than 1.6 million times. He is the cofounder and the Chief Scientific Officer at pureLiFi Ltd. He holds 31 patents and has more than 30 pending patent applications. He has published 300 conference and journal papers including a paper in Science. His main research interests include optical wireless communications, hybrid optical wireless and RF communications, spatial modulation, and interference coordination in wireless networks. He first introduced and coined spatial modulation and Li-Fi. Li-Fi was listed among the 50 best inventions in TIME Magazine 2011. He is a co-recipient of the best paper award at the *IEEE Vehicular Technology Conference* in Las Vegas in 2013 and in Glasgow in 2015. In 2012, he was the only one who received the prestigious Established Career Fellowship from the Engineering and Physical Sciences Research Council (EPSRC) within Information and Communications Technology in the U.K. He received the Tam Dalyell Prize 2013 awarded by the University of Edinburgh for excellence in engaging the public with science. In 2014, he was selected by EPSRC as one of the ten Recognizing Inspirational Scientists and Engineers Leaders.